MDPI

Article

Structural design of the wing for URCUNINA (UAV)

Juan Sebastian Pinto Delgado [1,†,‡], Hernan Dario Ceron [1,‡ 2,*]

[1] Mechanical Engineering student; juanpintod@usantotomas.edu.co
[2] USP Professor; hernan@sc.usp.br
‡ These authors contributed equally to this work.

Version January 7, 2019 submitted to Journal Not Specified

Abstract: The structural design of the wing for URCUNINA (UAV) was carried out. The preliminary design was conducted using aerodynamic restrictions to pass into a detailed design by a structural analysis. For this porpoise CFD simulations were accomplish to obtain the loads over the wing, the usage of a process to transform the CFD output into information that could feed the FEA model was accomplished. This process include data collection, Matlab extrapolations, polynomial fits and construction of the V-n diagram to obtain proper data that work as input for the FEA. The analysis was done in the software ABAQUS CAE. The comparison of 3 different configurations of layup give the tools to decide the configuration used as a proposal after being evaluated using displacements and failure theories.

Keywords: Structural-Design, Wing, Composite, Abaqus, Layup, FEA, Tsai-Wu

1. Introduction

The American continent is characterized by a pronounced mountainous geography, where a high number of active volcanoes represent a considerable risk for the communities near to them [1]. The supervision of these volcanoes is carried out by means of seismographs and other instruments that measure the seismic activity recorded by the tectonic plates, magma movement and increases in electromagnetic measurements that are what trigger an eruption [2]. These measurements or data obtained by the experts serve to make a reading of the state of the volcano and to prevent future catastrophes, alerting the surrounding populations. The most common supervision involves performing continuous flights over the volcanic domes, putting the safety of the crew at risk [3] However, with technological advances, the risk of face-to-face inspections on volcanoes has been reduced by making use of satellite images and UAVs (Unmanned Aerial Vehicles) that can supply images in real time and sensor data without exposing crew [4]. The School of Engineering of São Carlos at the University of São Paulo in Brazil, in its department of Aeronautical Engineering, has developed the project called URCUNINA-UAV, which has the purpose of aerial surveillance. The preliminary design of the aircraft was already done and and the main results are presented in Bravo-Mosquera [1].Currently, the URCUNINA-UAV is in its structural design phase. Therefore, in this work is presented the structural design of the UAV's wings in order to guarantee the manufacture and operation of the UAV in this sort of specific mission.

1.1. Materials

The aluminum has been used throughout the aeronautical history, mainly thanks to its high relation of strength, cost and weight which in the aeronautical area is a decisive factor due to the restrictions of take-off and maneuverability.
Currently, that perception has changed. New metal alloys have been introduced, in addition to

composite materials such as carbon-fiber, glass fiber and aramid, which enhance aircraft performance and reduce maintenance costs. [5],[6],[7],[8]

Composites materials have two or more organic or inorganic materials as explain in [9], their structure is based in two parts: The matrix in the composite structures works as the main medium that receive the reinforcement to increase strength. The matrix can be of two natures, organic like the Epoxy, Vinyl, SPM and inorganic like cement, concrete, metal and ceramics, The fibers are the most important structure in the composite on account due to they give the strength by reinforcing the matrix in the direction of lamination increasing the stress resistance. In addition, fibers can be oriented in several directions, granting different properties.
Some examples of fibers are: glass, carbon, cellulose, aramid, silicon carbide [10].

1.1.1. Carbon Fiber

The main composite used in the aeronautical industry is the CFC (Carbon Fiber Composite) due to the properties like weight and strength ratio which increase the performance of aircraft, as well the cost. Another advantages include part reduction, complex shape manufacture, reduced scrap, improved fatigue life, design optimization, and generally improved corrosion resistance. [11]
The manufacture of CFC aircraft components is generally done in three steps: first a mold of the component is layered with composite material according to the design specifications. Once the component is laid-up on the mold it is enclosed in a flexible bag tailored approximately to the desired shape. The assembly is enclosed usually in an autoclave, a pressure vessel designed to contain a gas at high pressures generally up to 1.5MPa raising the internal temperature to cure the resin [5].

Properties of a carbon fiber composite in different strengths and directions can be found in Table (1).[9]

	M6/SC1081	AS4/3501-6
Vf	0,65	0,63
ρ [g/cm^3]	1,6	1,58
$E_1[MPa]$	177x10^3	142x10^3
$E_2[MPa]$	10,8x10^3	10,3x10^3
$G_12[MPa]$	7,6x10^3	702x10^3
v_12	0,27	0,27
v_21	0,02	0,02
$F_1t[MPa]$	2860	2280
$F_2t[MPa]$	49	57
$F_6[MPa]$	83	71
$F_1c[MPa]$	1875	1440
$F_2c[MPa]$	246	228
ϵ_1t	0,016	0,015
ϵ_2t	0,005	0,006

Table 1. Properties of CFC taken from [Isaac M. Daniel and Ori Ishai, Engineering Mechanics of Composite Materials, Oxford University Press, New York, Second Edition, 2006.]

The challenge of using composite materials is the cost of producing it, the philosophy of design, reparability, inspection, dimensional tolerance and try to break the conservatism in the process as proposed in [5].

1.2. Theories of failure

A big variety of theories of failure exist and depend of the properties of the material, the theories are used to determine the safety of the structure that is submitted to stress [12].

When talk about theories of failure the most famous for isotropic materials are :

- Von-mises: The von Mises yield criterion suggests that the yielding of materials begins when the second deviatory stress invariant J2 reaches a critical value. It is part of a plasticity theory that applies best to ductile materials, such as some metals. Prior to yield, material response can be assumed to be anything i.e. nonlinear elastic, viscoelastic or simply linear elastic.

- Tresca: The Tresca yield criterion is taken to be the work of Henri Tresca. It is also known as the maximum shear stress theory (MSST). In terms of the principal stresses, this theory applies best to brittle materials and exclusive for isotropic materials.

In the non isotropic materials analysis exist theories like Tsai-Wu, Maximum-Stress, Max-Strain and Tsai-Hill wich are called the iterative category.

1.2.1. Tsai-Wu

The Tsai-Wu criteria is one of the most relevant in the iterative category. It pretends to generalize the failure criteria of Tsai Hill.
This criterion is based on the theory of plasticizing of an-isotropic materials of Hill that in the same way is based on the Von-misses criteria for isotropic materials [12],[9]. In a graphical way, the Tsai-Wu criteria is an ellipse with the principal stresses in the axis following the expression and showed in the figure (1) :

$$F_i\sigma_i + F_ij\sigma_i\sigma_j = 1 \tag{1}$$

In the simplified way, with the assumptions of 2D and only plain stresses

$$F_1\sigma_1 + F_2\sigma_2 + F_6\sigma_6 + F_11\sigma_21 + F_22\sigma_22 + F_66\sigma_66 + 2 * F_12\sigma_1\sigma_2 = 1 \tag{2}$$

The coefficients of the equation (2) are calculated with the following expressions that are properties of the material.

$$F_1 = \frac{1}{\sigma_{1t}} - \frac{1}{\sigma_{1c}}\ ;\ F_2 = \frac{1}{\sigma_{2t}} - \frac{1}{\sigma_{2c}}\ ;\ F_3 = \frac{1}{\sigma_{3t}} - \frac{1}{\sigma_{3c}}\ ;\ F_4 = F_5 = F_6 = 0$$

$$F_{11} = \frac{1}{\sigma_{1c}\sigma_{1t}}\ ;\ F_{22} = \frac{1}{\sigma_{2c}\sigma_{2t}}\ ;\ F_{33} = \frac{1}{\sigma_{3c}\sigma_{3t}}\ ;\ F_{44} = \frac{1}{\tau_{23}^2}\ ;\ F_{55} = \frac{1}{\tau_{31}^2}\ ;\ F_{66} = \frac{1}{\tau_{12}^2}$$

2. Urcunina (UAV)

The project Urcunina (UAV) is an initiative of the EESC (Escola de engenharia de São Carlos) the objective is to design a UAV to make supervision and monitoring of volcano's.
The Aerodynamic design is already developed which give to the next stage (structural) restrictions and data for the design. The geometry, restrictions and characteristics are going to be presented.
In the figure (2) are defined the design requirements of the UAV, based in those requirements the

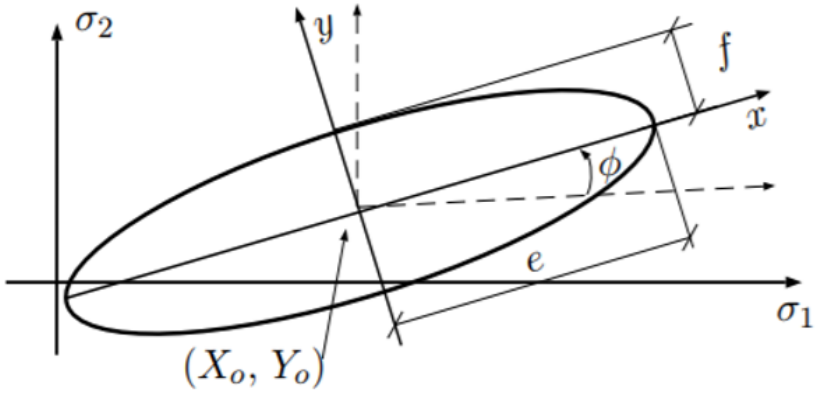

Figure 1. Tsai- Wu criteria

aerodynamic group design the geometry, airfoils, configurations, propulsion as obtained in [1].

Flight	Payload	Aerodynamic	Structural
Take-off altitude = 2527 m	Mass spectrometer	High Lift	Wood and carbon fibre
Operational altitude ≈ 4300 m	Avionics	Low Drag	Monitoring temp. ≈ −8 °C
Service ceiling ≥ 4500 m	Batteries	Low Re	Combustion Engine + Ash filter
Range ≥ 20000 m	Optical sensors	High wing	
Endurance ≥ 4 h	IR sensors	V-inverted tail	
Payload = 4 kg	Parachute	Pusher configuration	
Monitoring velocity ≈ 20 m/s			
Cruise velocity ≈ 28 m/s			

Figure 2. General characteristics of Urcunina

2.1. Geometry

The geometry of the UAV is given from the aerodynamical design [1], these design accomplish with the aerodynamic objectives and some of the structural ones.

The UAV have a standard fuselage in which the main purpose of it it's to carry out the payload that are the instruments to make the inspection of the volcano. The wings have a standard configuration of trapezoidal wings in a high mount position with an airfoil Eppler 423 high lift.
In the figure(3) are shown the features determined by the aerodynamic group also in figure (4,5,7,(8) are showed a frontal, plant, lateral and a isometric view of URCUNINA. [1].

Wing features.

Wing Parameters	Value
Wingspan (b)	2.9 [m]
Root chord length (C_r)	0.348 [m]
Tip chord length (C_t)	0.174 [m]
Mean aerodynamic chord	0.27 [m]
Wing Area (S)	0.75 [m^2]
Angle of sweep $\Lambda_{c/4}$	0°
Airfoil thickness t/c	0.125
Aspect Ratio (AR)	11
Washout angle	1°
Operational Lift Coefficient	0.906
Maximum Lift Coefficient	2
Oswald efficiency (e)	0.98
Aerodynamic Efficiency	23.3
Airfoil	EPPLER 423

Figure 3. Urcunina wing features

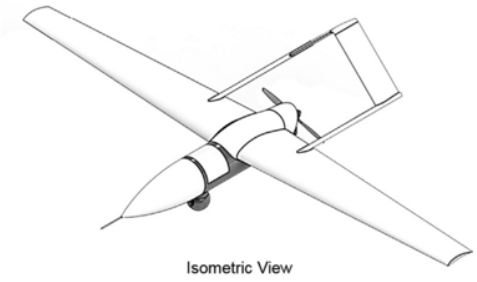

Figure 4. Urcunina isometric view

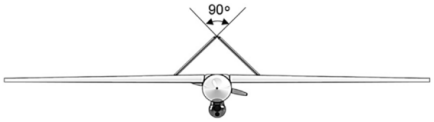

Figure 5. Frontal view Urcunina

In the empennage the Inverted-V configuration was adopted, and joined to the fuselage by Tail-booms and have a NACA 0012 airfoil [1]. In the next table are presented the features determined by the aerodynamic group.

Empennage features.

Empennage Parameters	Value
Empennage span (b_e)	0.6 [m]
Chord length (c)	0.160 [m]
Empennage area (S_e)	0.1042 [m^2]
Empennage volume (V_e)	0.052 [m^3]
Airfoil thickness t/c	0.12
Aspect Ratio (AR)	3.75
Angle of incidence	0°
Airfoil	NACA 0012

Figure 6. Empennage features

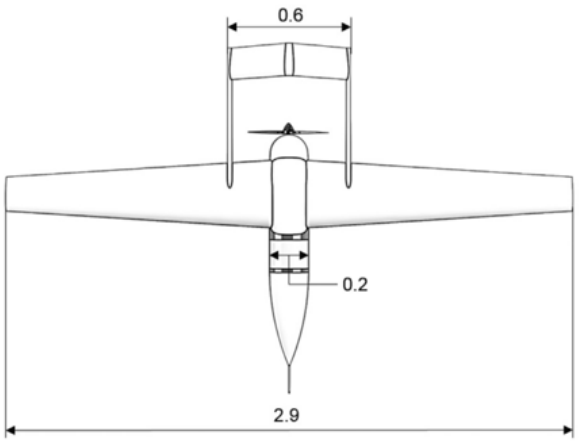

Figure 7. Plant view

For the propulsion it was selected an internal combustion engine due to the endurance, capabilities and cost compared to an electrical one [1]. The 3w-28iCS engine was adopted and

equipped with an ash filter, the characteristics of the engine are:

- 28.5 cm^3 of Vf with an only stroke
[1]
- Static thrust of 16 kg

-Rotational field 1500-8500 RPM

- Nominal Power: 2.65 kW (3.6 Hp)

- Weight of 1.2 Kg

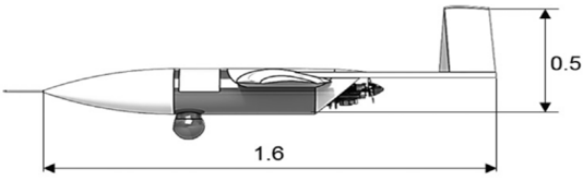

Figure 8. Lateral View

3. Structural analysis

In this stage of the document will be talked about the structural analysis of the UAV and all the tools involved in the development of the model and the results. First of all is important to mention that all the analysis and model will be done by the Finite Element Method.

3.1. Finite Element Method (FEM)

The finite element method is one way to simplify complex systems in order to obtain approximate solutions when it's too difficult to obtain an analytical solution.

The description of the laws of physics for space- and time-dependent problems are usually expressed in terms of partial differential equations (PDEs). For the vast majority of geometries and problems, these PDEs cannot be solved with analytical methods. Instead, an approximation of the equations can be constructed, typically based upon different types of discretization's. These discretization methods approximate the PDEs with numerical model equations, which can be solved using numerical methods. The solution to the numerical model equations are, in turn, an approximation of the real solution to the PDEs. The finite element method (FEM) is used to compute such approximations [13].

As the names says the idea is to make division into elements that are more simply to analyze, the models can be complex or simple, can be in 2d or 3d it will only change the complexity, time, resources and modeling [14].

In the FEM you can variate the quality of the results by making more discretization of the elements that results in more elements, more time, more resources but can give a better result, these type of improve in the model usually is given in zones which the gradients of stresses can be crucial in the design as its described in [8].

The elements are classified in various types and it could be read a better description in [5]

In the FEA analysis of layup composites is used the planar elements of shell type due to the capability of represent the stresses and deformation characteristics of the material, for the URCUNINA analysis is used this type of element.

Shell or Plate Elements: Shell elements are used to model thin 3D structures usually acted upon by bending type loads. This element uses a different stiffness formulation than a standard solid element allowing higher accuracy.
[13]

3.2. Abaqus

Abaqus FEA (formerly ABAQUS) is a software suite for finite element analysis and computer-aided engineering, originally released in 1978. The Abaqus suite is used to develop the FEA analysis of the URCUNINA wing structure .

It's really important to say that in Abaqus the software does not works with a system of units, the user can't define a unified system, is important to introduce the units accurate to obtain appropriate results. For example, to work in SI is required to insert length in [mm], loads in [N], young module in [MPa], area in $[mm^2]$ [5].

The unit consistency it's really important.
Every complete finite-element analysis consists of 3 separate stages:

- Pre Processing
- Analysis
- Post Processing

4. Structural modeling of Urcunina wing in Abaqus

4.1. Geometry

From previous works [1], the geometry of the wing was obtained. The geometry of the Urcunina wing is presented in the figures (9,10,11).

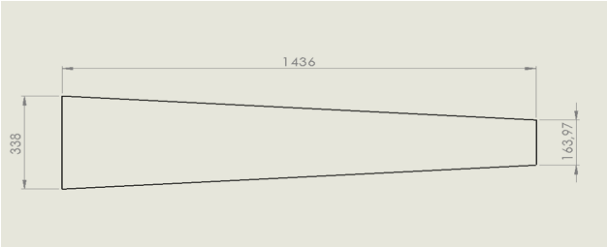

Figure 9. Plant view of the wing

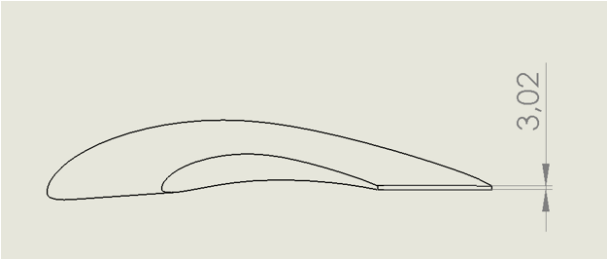

Figure 10. Lateral View of the wing

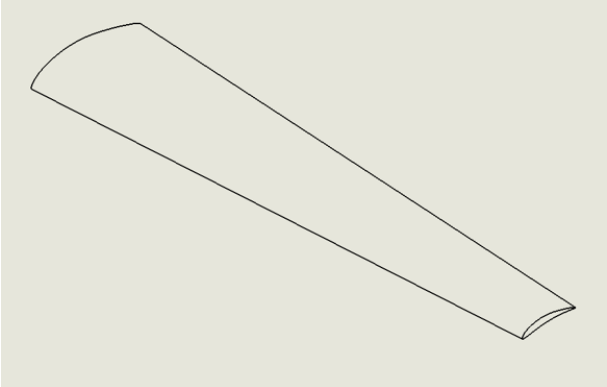

Figure 11. Isometric view of the wing

Due to the fact that the material of the design is a composite laminated the wing is modeled as a shell finite element.

The spar was allocated at the maximum thickness airfoil in order to grant a largest height spar. The maximum thickness of the airfoil is located at the 23.7 % of the chord and the maximum curvature is located at the 41.4 % [1].

Also the other principal substructure of the wing are the ribs which distribution aims to allocate the control surfaces. There are two groups of ribs as presented in figure (12). The inner group are responsible of the aerodynamical shape and a proposal for the fuselage-wing joint in the root rib; the outer group, besides the aerodynamic characteristics are the base for the aileron location.

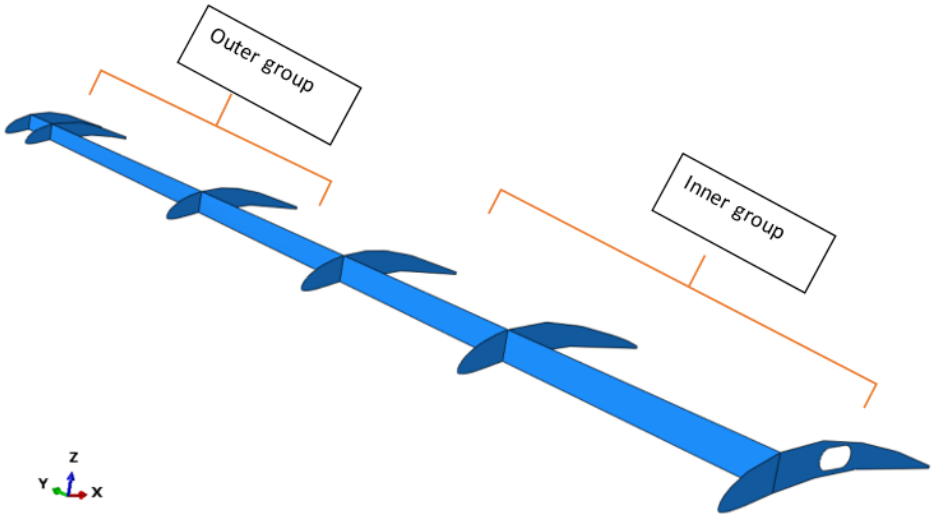

Figure 12. Principal spar and ribs distribution

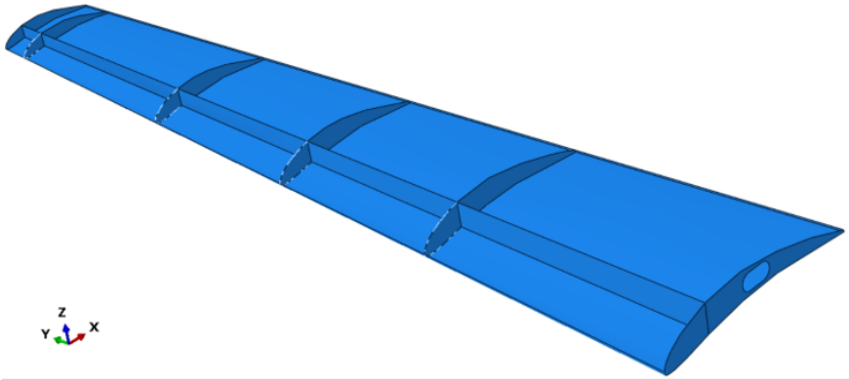

Figure 13. Top skinless Isometric view of the model in Abaqus

As showed in the figure (13) the model has been divided into two surfaces the Upper surface and the Lower surface in order simplify the laminating process. Finally, after the aerodynamic analysis and specification of the control surfaces localization the geometry used to the structure analysis is showed in the figure (14).

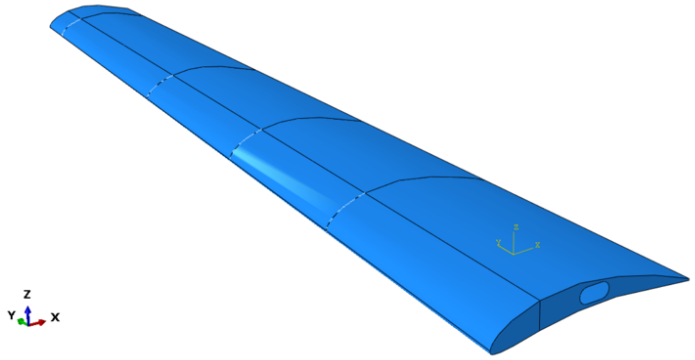

Figure 14. Urcunina geometry model

4.2. Material

As mentioned before the material of design of the UAV is the CFC (Carbon Fiber Composite) M6/SC1081, more specific is a Carbon-epoxy material with properties in Table (1).

The material have been chose due to the research in the Daniel Ishai bibliography of composites [9].

The material is defined in the software as lamina with elastic properties. The orientation of the ply will help the structure to handle the specific stresses that the different zones of the wing have to endure, not all the structures and substructures have the same porpoise, most of them are designed to work under specific loads situations granting the better results.

As part of the analysis it will be 3 different configurations in different layups in order to grant the lightest and resistant structure as the design parameters allow it.

The first configuration is a classical layup that contain 4 layers which orientation are result of the research in papers, books and consults, the orientations and details are include in the table (2).

Region	Material	Thickness [mm]	Rotation angle
A (upper- lower surface)	Carbon-epoxy	0,25	[0/45/-45/0]
B (Spar)	Carbon-epoxy	0,25	[0/45/-45/0]
C (Rib)	Carbon-epoxy	0,25	[0/90/0/90]

Table 2. Orientations of the layup for the configuration # 1

The second configuration is equal to the first one but with a layer removed to check the weight, stresses, deformations and displacements behaviors,the orientations and details are include in the table (3).

Region	Material	Thickness [mm]	Rotation angle
A (upper- lower surface)	Carbon-epoxy	0,25	[0/45/0]
B (Spar)	Carbon-epoxy	0,25	[0/45/0]
C (Rib)	Carbon-epoxy	0,25	[0/90/0]

Table 3. Orientations of the layup for the configuration # 2

The last configuration is a 4 ply layup that mix layers of 45 ° and 90 ° orientation as showed in the table (4)

Region	Material	Thickness [mm]	Rotation angle
A (upper- lower surface)	Carbon-epoxy	0,25	[0/45/0/90]
B (Spar)	Carbon-epoxy	0,25	[0/90/0/90]
C (Rib)	Carbon-epoxy	0,25	[0/90/0/45]

Table 4. Orientations of the layup for the configuration # 3

For a better comprehension of the configurations and the 3 regions that will change the layup, according to the tables above mentioned, in the figures (15,16,17) are presented separately.

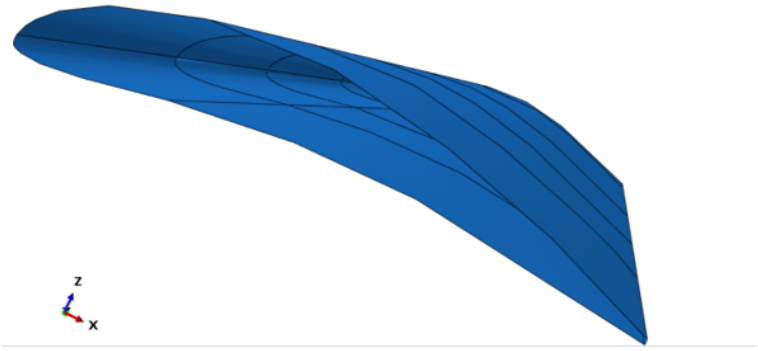

Figure 15. Region A (Upper surface, Lower surface)

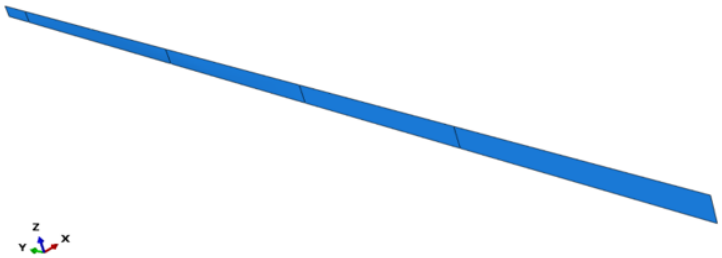

Figure 16. Region B (Spar)

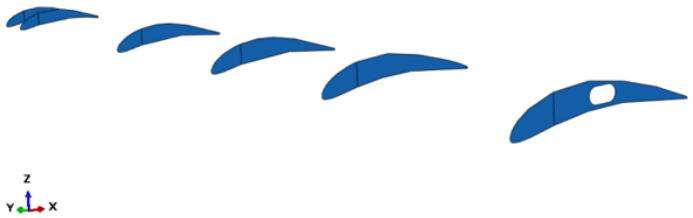

Figure 17. C (Ribs)

222 *4.3. Mesh*

223 The analysis was carried out by the Finite Element Method (FEM) then it was necessary to
224 discretize the domain to generate a mesh in order to obtain an approximation to the solution of the
225 differential equations.

226

227 The ideal FEM mesh for a shell element is a mesh with only shell (quad4) elements which are able
228 to represent all stress states including bending. However, due to the complexity of the geometry some
229 triangular elements are generated [8].

230

231 From the original geometry, the mesh seed is generated and submitted to a series of quality
232 analysis in order to obtain the final mesh. The figure (18) shows the mesh in an isometric view, note
233 that the T.E was truncated.

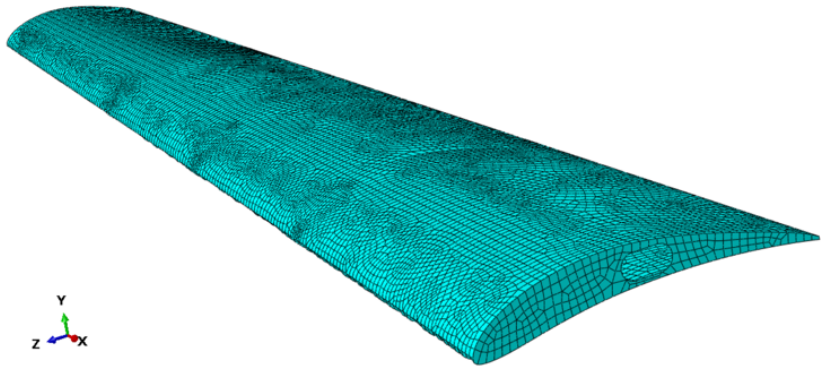

Figure 18. Isometric view of the mesh

234 The figure (19) presents the internal sub-structures of the wing mesh, as can be seen in the spar
235 thanks to the rectangular shape the mesh is a structured quad4 mesh that make the transition into the
236 ribs geometry improving the generation of quad4 elements despite of the curve geometry.

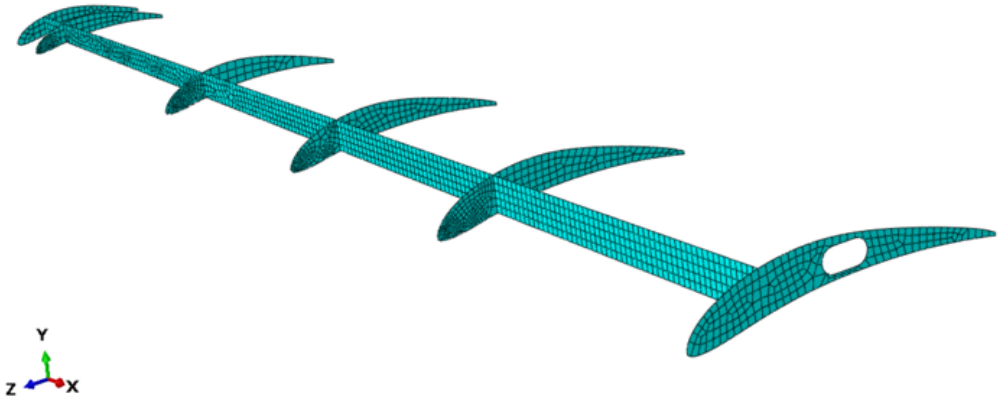

Figure 19. Internal structures mesh

As the T.E was truncated, its geometry grant that the mesh will continue the shell (Cquad4) element and there are no triangular elements.

Number of Elements (total)	18753
Upper surface	7503
Lower surface	8720
Ribs	1630
Spar	900

Table 5. Number of elements in the mesh

4.4. Boundary Conditions

The boundary conditions that was applied to the model is encastre (Fix) in the principal spar as well as in the root rib. This condition was applied to grant the worst case scenario of the joint wing-fuselage [14].

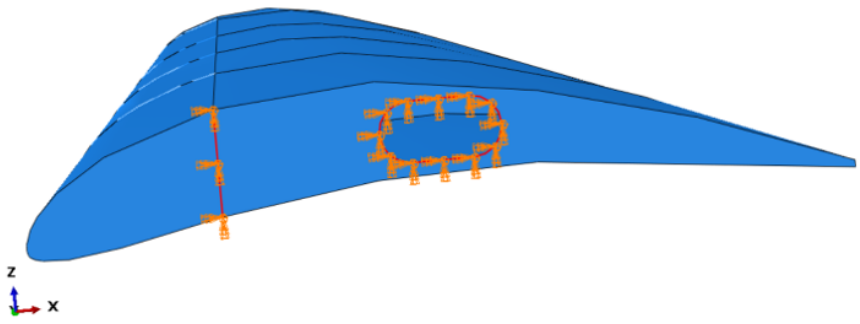

Figure 20. Encastre boundary condition

4.5. Loads

4.5.1. V-n Diagram

The V-n diagram it's a graphical way to determine structural limits, it's a diagram in function of the speed of the fluid.

The model used to estimate the load factors (n) it is an approximation for lightweight airships in a low Reynolds regime. It is also based in the aeronautical legislation and determined due to the weight characteristics and the lift distribution, an example is presented in the figure (21) obtained from the FAR-23. [15]

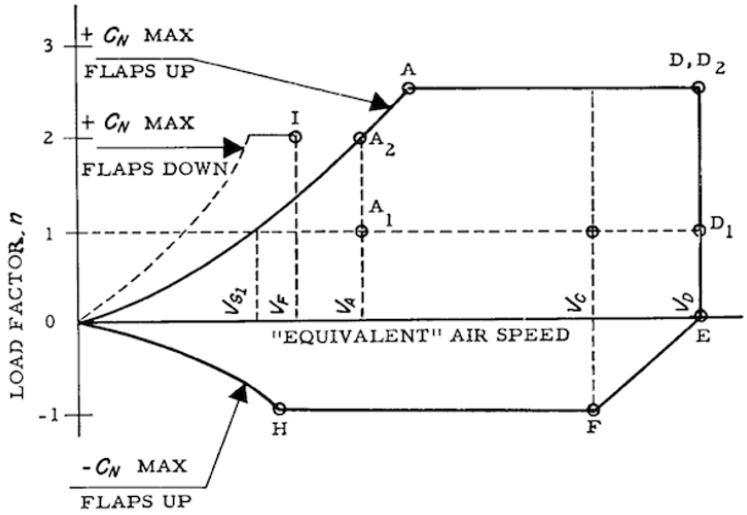

Figure 21. V-n diagram structure

$$n = \frac{\rho V^2 S C_L}{2W} \tag{3}$$

The equation(3) is the mathematical expression to obtain the value of n (load factor) of the aircraft in different typical situations. Where :

ρ = Density of the fluid
v = Speed of the fluid
S = Superficial Area of the Wing
W = Weight of the plane
C_L = Lift coefficient

Using the analytical process explained in [15] is obtained the V-n Diagram for the Urcunina operation as well as the gust diagram and the final diagram that is the graphical representation of the structural limits of the airship in operation. These n factors will be applied into the model to include the acceleration effects and safety factor.

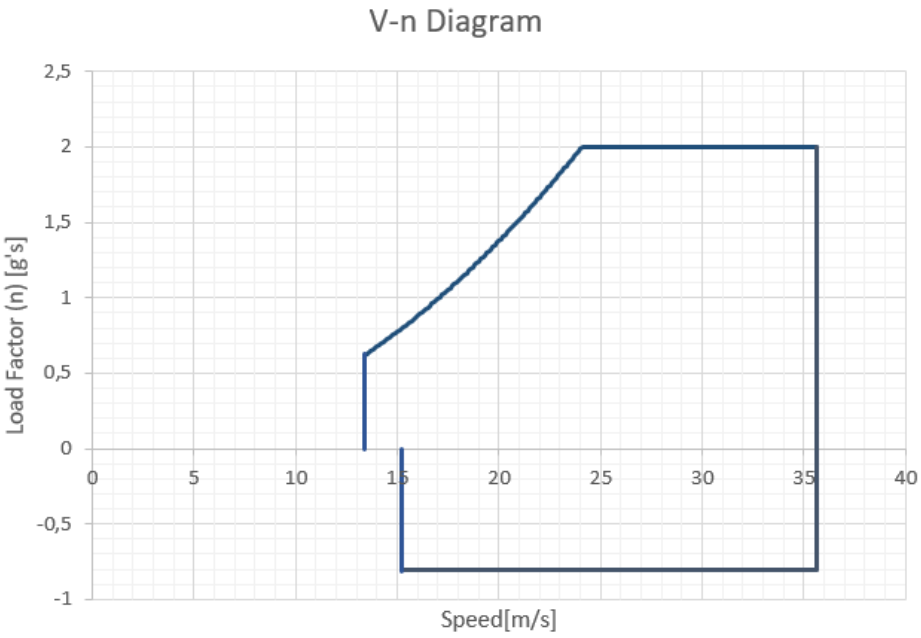

Figure 22. Operation V-n diagram

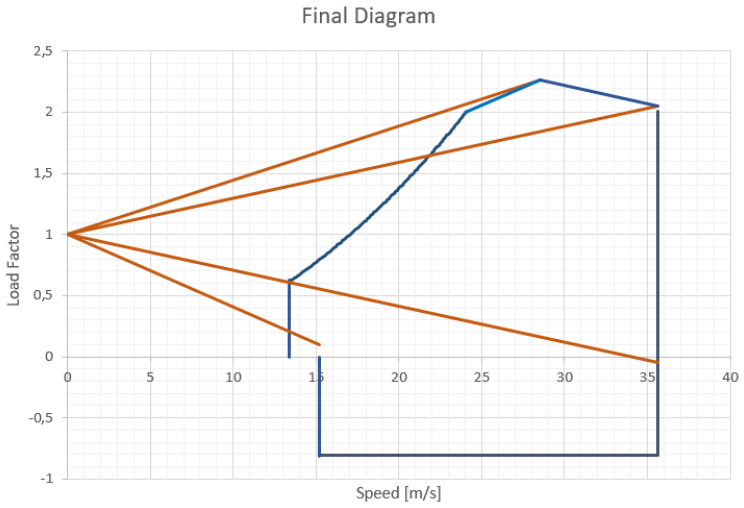

Figure 23. Final Urcunina V-n diagram

The figures (22,23) present the V-n diagram and the final diagram of URCUNINA operation and presents relevant data e.g the situation where the structure could suffer the most critical behavior. This critical situation will be in the gust at Cruise Speed then for this situation the structural analysis was conducted (n=2.26).

In the table (6) is showed the relationship of the n value with the speed in the final diagram.

Situation	n Factor	Speed [m/s]
Stall +	0.624	13.4
Stall -	-0.81	15.2
Operation	2	24
Cruise	2.26	28.5
V_d	2.05	35.6

Table 6. n values from V-n diagram

C_L is obtained by equation (4)

$$L = 1/2\rho V^2 C_L s = nW \tag{4}$$

where :
ρ , Density of the air in operation
V, Speed of the wind
S, Area of the wing
N, Load Factor W, Weight of the aircraft
ρ =0.8 $[kg/m^3]$
n =2.26
S=0.75 $[m^2]$
V = 28.5 [m/s]
W= 147.15 [N]
The weight estimation is obtained by the restriction of MTOW reported in [1]
The value of CL=1.36 was obtained with the above data.

4.5.2. CFD approach

Computational Fluid Dynamics (CFD) simulations were computed in order to determine the pressure distribution along the wingspan that corresponds to C_L=1,36. The goal of the aerodynamic analysis is to obtain the aerodynamic loads that must support the wing in function of some critical condition of the URCUNINA-UAV mission. Thus, CFD simulations were performed using the commercial code ANSYS – CFX software (release 14.5), solving Reynolds Average Navier-Stokes (RANS) equations. The turbulent flow was modeled by standard Shear Stress Transport (SST) model, at which the governing equations were discretized by a second-order scheme.
Computational Domain

The size of the computational domain was created by ensuring the flow around the wing is not affected by the boundaries of the fluid domain. A computational sub-domain was designed in order to reduce the size of the elements near the walls of the wing, aiming to obtain a better numerical accuracy on this region. Figure (24) shows the computational domain created for the numerical simulations, presented as a function of the root chord length (C).

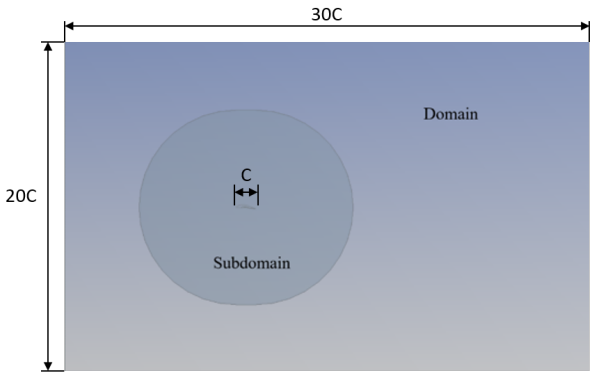

Figure 24. Computational domain

Grid strategy

A multi-block unstructured grid was generated using ICEM-CFD, which is composed by tetrahedral cells for all computational domain and prism cells for capturing the boundary layer effects on the walls near the model (Fig. 26). It is composed by 15 layers, whose first layer of cells was set at 2.1×10^{-4} m from the configuration wall, resulting in a Y^+ equal to 1. This grid was computed after an independence mesh analysis which aids to guarantee that the element size does not affect the results. Figure (25) shows the variation of the lift coefficient as a function of the number of nodes, where 9 several grids were assessed. The mesh independence study showed that the lift force converges at approximately 1693920 nodes.

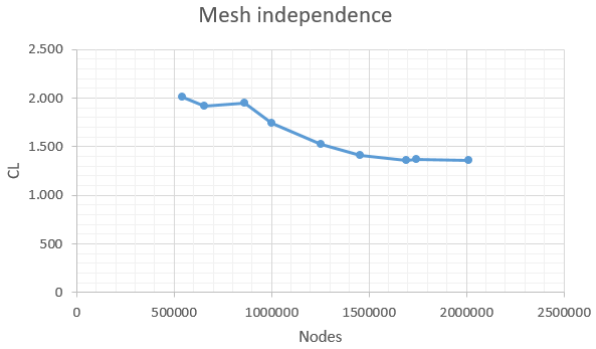

Figure 25. Mesh Independence

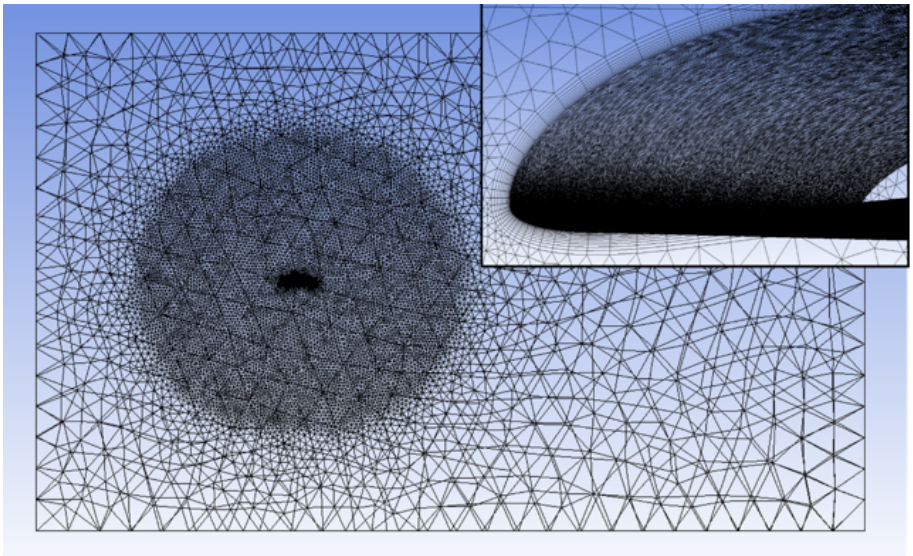

Figure 26. Computational mesh

Boundary conditions

Numerical simulations at steady-state condition were performed. The URCUNINA-UAV wing was simulated at the operating velocity of the aircraft and at angle of attack equal to 5.5 [deg], which corresponds to a lift coefficient equal to 1.36. This value was extracted from the limit gust envelope of the V-n diagram (n=2.26). The outlet boundary was imposed without pressure gradient. The wing was treated as no-slip boundary condition, whereas the far walls of the domain were imposed as free-slip boundary condition. Finally, at the half of the longitudinal plane of the wing, symmetry boundary condition was imposed. The convergence criteria reached a maximum residue of 1e-5, with exactly 400 iterations.

Post-processing

The required structural strength was taken from the pressure distribution using a polyline from the root to the tip with a step of 10% along the wingspan.

5. CFD to FEA

The output data from the CFD are transformed to set up the FEA model. The input data are the values of pressure along chordwise for 11 stations on the spanwise direction.

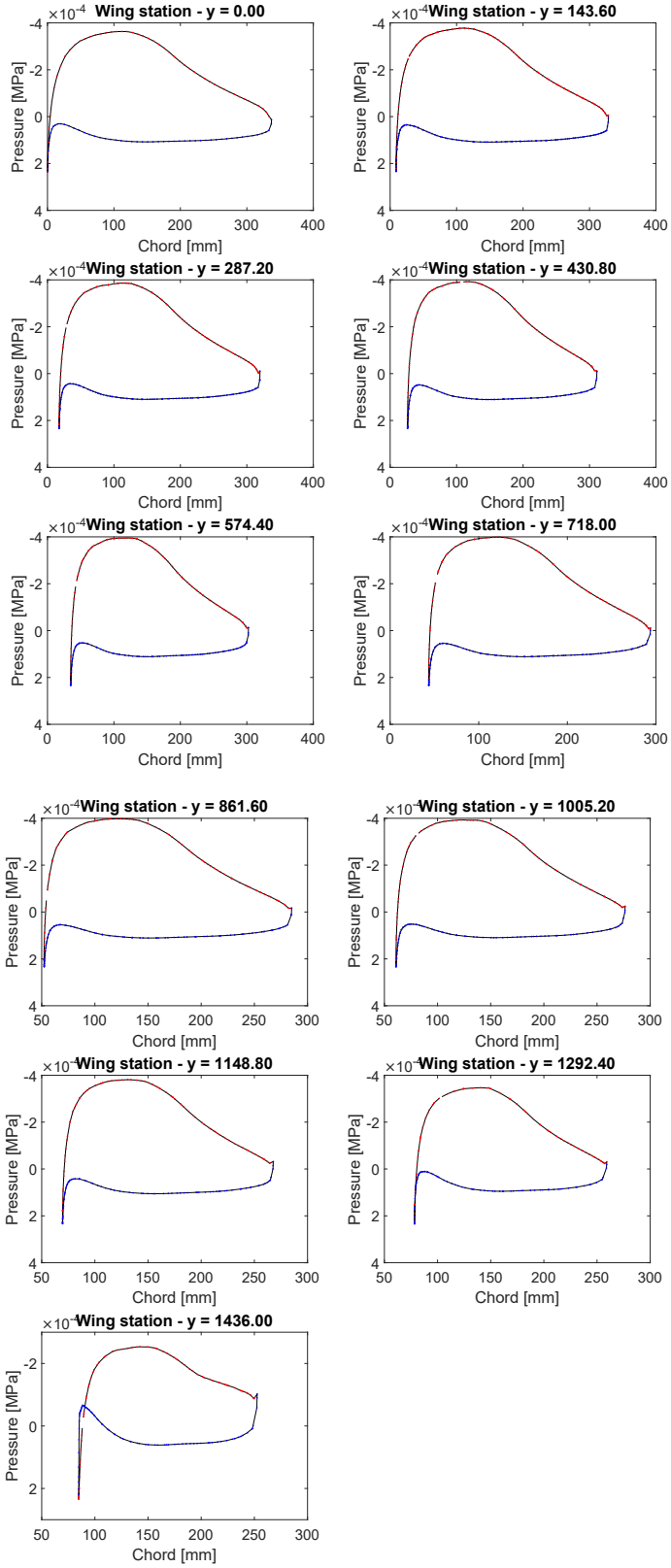

Figure 27. Pressure stations along the wing

These stations provide the wing load estimation both the upper and lower surfaces., in the figures (28,29) is presented the input data.

Bear in mind that the negative pressure and the pick of suction are the main characteristic of the upper surface and therefor there is a favourable gradient pressure near to the leading edge on this surface.

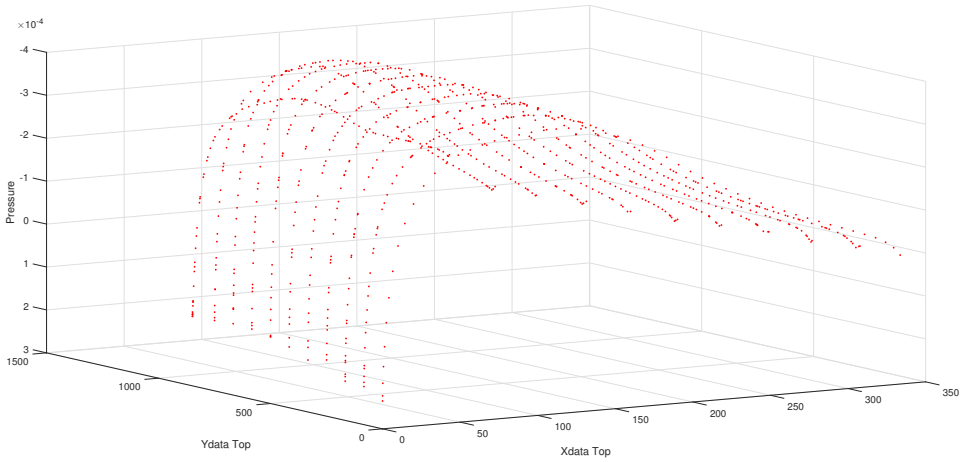

Figure 28. Upper surface pressure stations

In the figure (29) is showed the pressure data of the lower surface that represent the deceleration of the fluid.

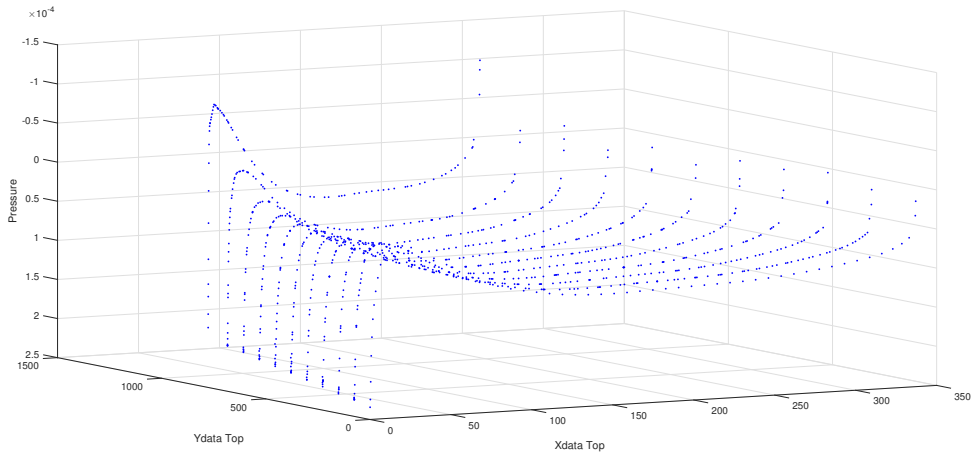

Figure 29. Lower surface pressure stations

In order to improve the analysis an interpolation of data is required to fulfill the spaces between the stations and get a whole surface that represent the loads in the wing.

Using Mat-lab software interpolation was done and is presented in figures (30,31). This figures gives to the analysis information of what is happening in the whole semi-span not just in sections.

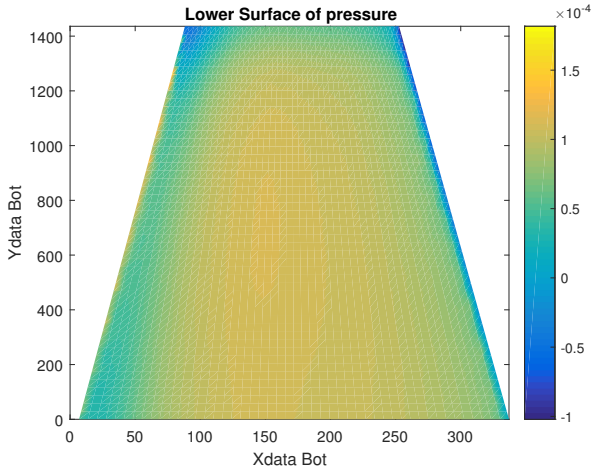

Figure 30. Lower pressure surface

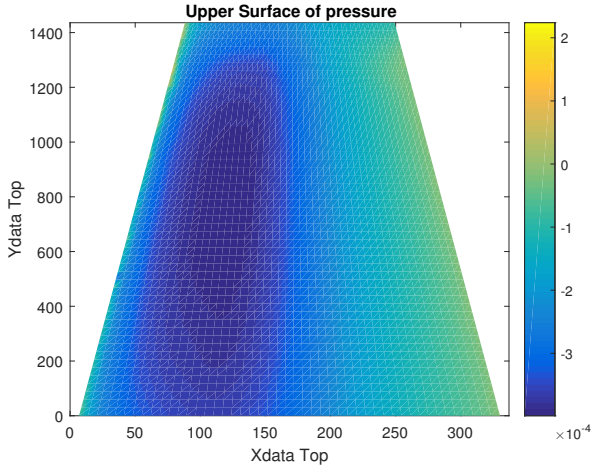

Figure 31. Upper pressure surface

The interpolated data is used to create a numerical fit with a polynomial expression that can be used in the FEA model. This process is done with the Mat-lab software .

For the Upper surface the fit is a polynomial expression of 5x4 which means the variable "X" goes until its 5 power and "Y" until the 4 the equation is presented in (5).

$$sf_{top}(x,y) = p00 + p10 * x + p01 * y + p20 * x^2 + p11 * x * y + p02 * y^2 + p30 * x^3 + p21 * x^2 * y$$
$$+p12*x*y^2 + p03 * y^3 + p40 * x^4 + p31 * x^3 * y + p22 * x^2 * y^2 + p13 * x * y^3 + p04 * y^4$$
$$+p50*x^5 + p41 * x^4 * y + p32 * x^3 * y^2 + p23 * x^2 * y^3 + p14 * x * y^4.$$

(5)

Coefficients (with 95 % confidence bounds):
p00 = 0.0001065 (9.009e-05, 0.000123)

p10 = -1.508e-05 (-1.617e-05, -1.398e-05)
p01 = 1.587e-07 (2.034e-08, 2.972e-07)
p20 = 1.765e-07 (1.55e-07, 1.98e-07)
p11 = -1.995e-08 (-2.318e-08, -1.671e-08)
p02 = 2.816e-09 (2.428e-09, 3.204e-09)
p30 = -9.754e-10 (-1.142e-09, -8.089e-10)
p21 = 2.476e-10 (2.136e-10, 2.816e-10)
p12 = -3.598e-11 (-4.017e-11, -3.178e-11)
p03 = -1.44e-12 (-1.851e-12, -1.029e-12)
p40 = 2.715e-12 (2.16e-12, 3.271e-12)
p31 = -1.025e-12 (-1.17e-12, -8.794e-13)
p22 = 1.421e-13 (1.223e-13, 1.62e-13)
p13 = 1.024e-14 (7.392e-15, 1.309e-14)
p04 = 6.252e-16 (4.8e-16, 7.705e-16)
p50 = -2.954e-15 (-3.621e-15, -2.288e-15)
p41 = 1.389e-15 (1.176e-15, 1.602e-15)
p32 = -1.848e-16 (-2.195e-16, -1.502e-16)
P23 = -1.189e-17 (-1.698e-17, -6.796e-18)
p14 = -3.219e-18 (-4.042e-18, -2.396e-18)

This coefficients represent the values will adopt the variables in the expression to result in the fit surface.

The equation (5) results in the surface that is presented in figure (32) that include the interpolation data.

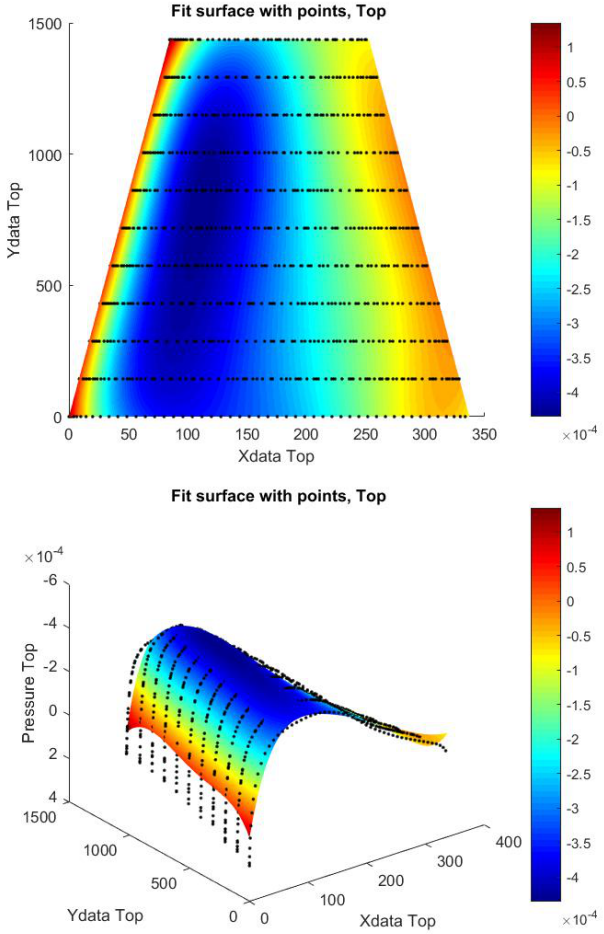

Figure 32. Upper surface load fit

For the selection of the degree of polynomial fit it was concluded an error study taking into account the Maximum and Medium error for all the possible combinations in the power values.

In the lower surface the process was similar which results in a 5X5 polynomial expression to fit the data.

The 5x5 polynomial expression is the following:

$$sf_{bot}(x,y) = p00 + p10 * x + p01 * y + p20 * x^2 + p11 * x * y + p02 * y^2 + p30 * x^3 +$$

$$\text{p21*x}^2 * y + p12 * x * y^2 + p03 * y^3 + p40 * x^4 + p31 * x^3 * y + p22 * x^2 * y^2 +$$
$$\text{p13*x*y}^3 + p04 * y^4 + p50 * x^5 + p41 * x^4 * y + p32 * x^3 * y^2 + p23 * x^2 * y^3 +$$
$$\text{p14*x*y}^4 + p05 * y^5 \quad (6)$$

Coefficients (with 95% confidence bounds):

p00 = 0.0001335 (0.0001233, 0.0001438)

p10 = -6.548e-06 (-7.263e-06, -5.833e-06)

p01 = 3.11e-07 (2.094e-07, 4.126e-07)

p20 = 1.393e-07 (1.252e-07, 1.534e-07)

p11 = -1.214e-08 (-1.426e-08, -1.003e-08)
p02 = 7.37e-10 (3.648e-10, 1.109e-09)
p30 = -1.07e-09 (-1.179e-09, -9.617e-10)
p21 = 1.129e-10 (9.071e-11, 1.352e-10)
p12 = -6.654e-12 (-9.356e-12, -3.951e-12)
p03 = -5.92e-13 (-1.201e-12, 1.698e-14)
p40 = 3.461e-12 (3.101e-12, 3.822e-12)
p31 = -3.576e-13 (-4.519e-13, -2.633e-13)
p22 = 1.08e-14 (-2.105e-15, 2.37e-14)
p13 = 4.049e-15 (2.229e-15, 5.869e-15)
p04 = 2.985e-16 (-1.507e-16, 7.478e-16)
p50 = -4.003e-15 (-4.432e-15, -3.573e-15)
p41 = 3.241e-16 (1.872e-16, 4.61e-16)
p32 = 2.471e-17 (2.327e-18, 4.71e-17)
p23 = -1.386e-17 (-1.718e-17, -1.053e-17)
p14 = 6.012e-19 (7.336e-20, 1.129e-18)
p05 = -1.588e-19 (-2.81e-19, -3.662e-20)

The equation (6) results is the surface in figure (33) including the interpolation data in the figure(33).

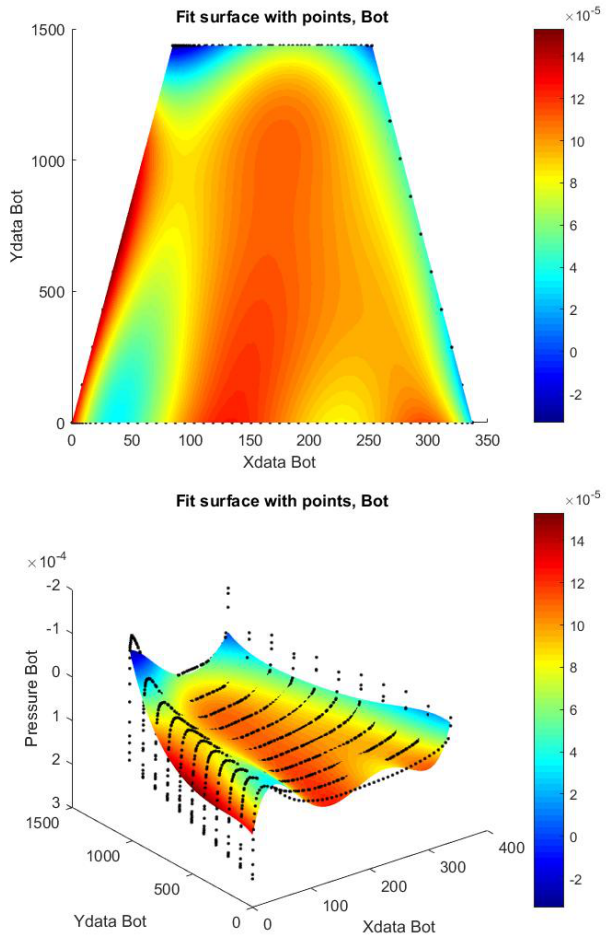

Figure 33. Lower surface load fit

The software Abaqus offer a tool to input loads to the model. That tool is to create an Analytic Field with a polynomial expression to represent the variation in the load through the wing.

Using the Analytic expression field in Abaqus the loads finally were introduced into the model. It is important to say that to the loads input was applied the load factor (n=2.26), as well as in the gravity force that results in the weight component showed in the figure (34).

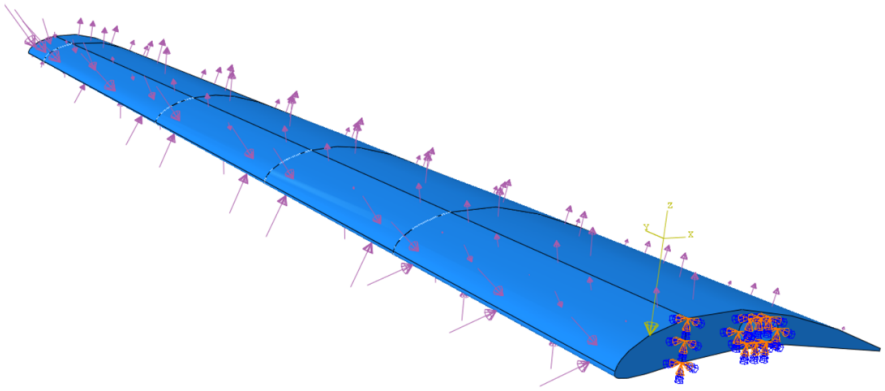

Figure 34. Final loaded model

After the final model its finished with geometry, material and loads the next step was to validate the different configurations of the layup.

As a design parameter the weight of the structure is a variable to take into account with each one of the layups configurations.

Configuration	Layers	$\rho[g/mm^3]$	W [N]	M [kg]
1	4	0.016	29.65	3
2	3	0.016	22.23	2.26
3	4	0.016	29.65	3

Table 7. Weights of the configurations

6. Results

In this section, the structural characteristics and numerical results of the analysis are presented, displacements and stresses.

6.1. Displacements

In the figure (35) is presented the results of displacements in the different directions of the model.

Using the U3 data presented in the figure (35) is obtained the deflection in the tip of the wing, where is maximum. To calculate the maximum deflection angle in the wing was used the following expression:

$$\theta = Tan((\Delta U_3)/Chord)^{-}1 \tag{7}$$

The $\Delta\ U_3$ is obtained by taking the U_3values in the attack edge and the trailing edge.
The results are showed in table (8) :

	Angle [°]
Configuration 1	0.07
Configuration 2	0.1476
Configuration 3	0.113

Table 8. Deflection angle

For this research, it is undertaken that the θ variation is small and therefore it will not be representative on a possible lift coefficient variation.

When looking into the U2 data is observable that in the configuration with only 3 layups the displacement in the radial axis is less than 1 [mm].

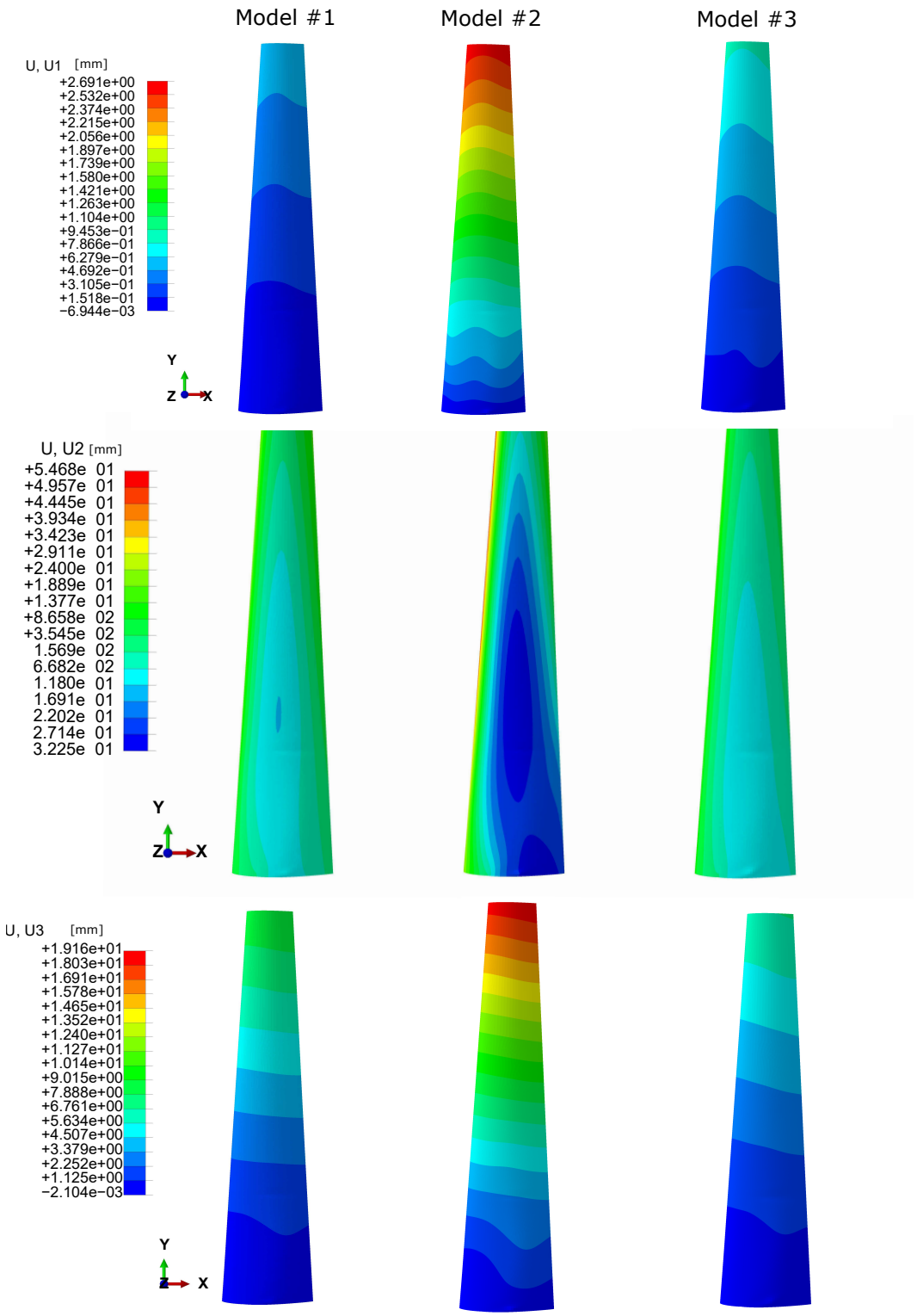

Figure 35. Top surface displacements

438 *6.2. Stress*

439 The stress results in this analysis will work as an indicator to decide between the 3 configurations.
440 When working with composite materials is important to take into account that the material does not
441 works as isotropic, which means that the properties does not have the same behavior in all directions.
442
443 The parameters of evaluation in the analysis will be the components S11 and S22 of the material,
444 which represent the stresses in the two principal directions of the composite layup, independent of the
445 angle of orientation.
446
447 Using the software Abaqus is possible to see the results in each ply, it will help to understand the
448 behavior of the composite structure, in the figure (36) is presented the distribution of the stress in the
449 principal axis S11, the figure is a bottom view (Lower surface) of stress in the principal direction of the
450 ply (S11).
451
452 In the figure it is visible the highest S11 stress as expected its located at the boundary condition
453 that represent the joint wing-fuselage. The figure help to understand how it is propagating the stress
454 in the principal axis of the different layers due to the angle of orientation.
455
456 Making a comparison with the second configuration that it's the same layup but taking off the
457 intermediate ply (-45 [°]) the difference is substantial in the distribution of the S11.
458
459 In order to make a comparison the figure (35) contain the three configurations showing the results
460 for the 3 models.
461
462 The configuration 3 even when it has 4 layers does not gives the best results. Taking a look to the
463 first configuration the maximum value of S11 is around the (274 [MPa]) and in the 3 configuration
464 goes 80 [MPa] above.
465

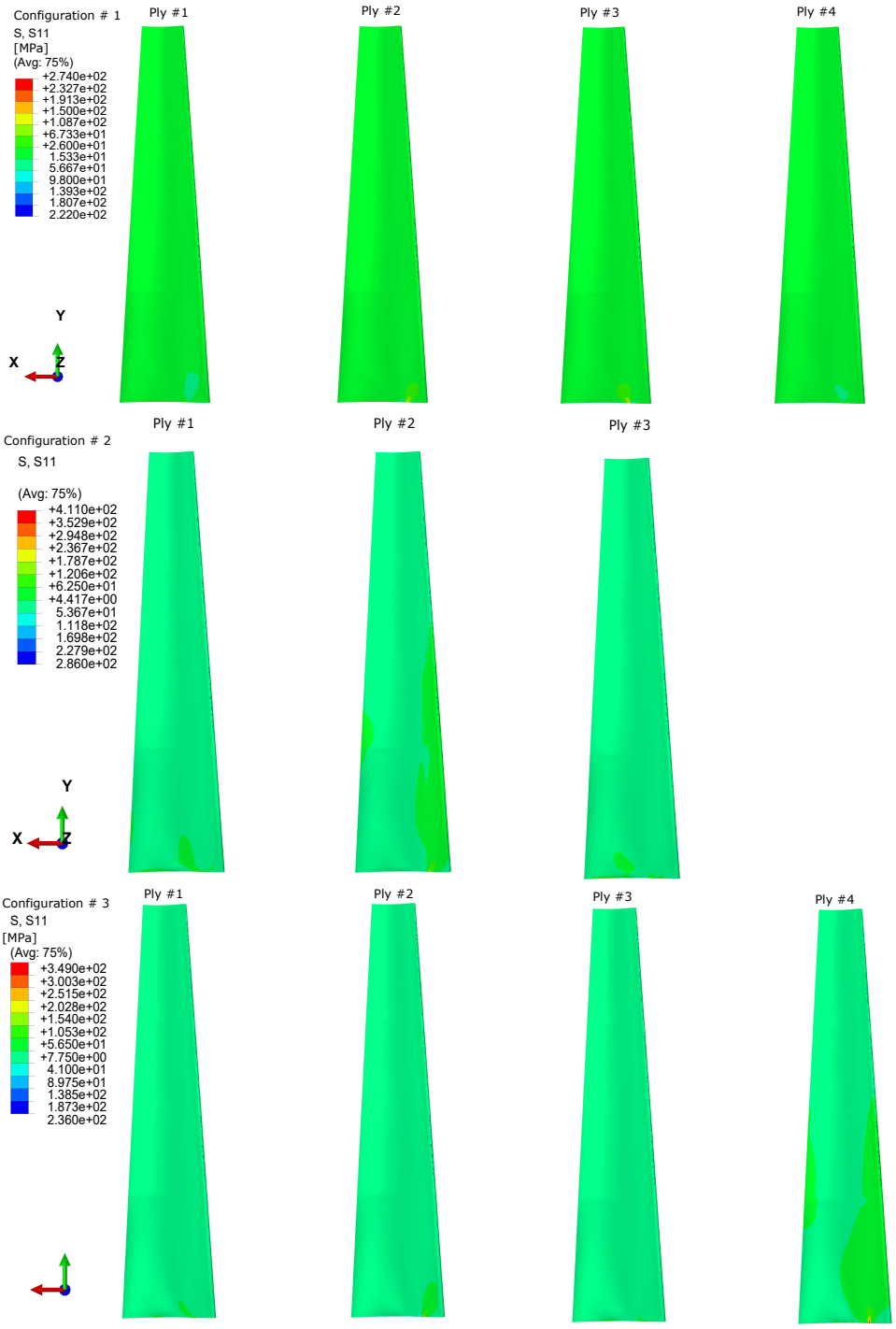

Figure 36. Stress S11 bottom surface

Even thought the 3 configurations are different among number of layers and orientation of plys the S22 stress does not have really big values and variations in comparison with S11. As it is going to be discussed in the next section the failure is generated due to the combination of S11,S22,S12 in all the nodes.

The figure (37) present contour plot's of the lower surface that represent the values of S22 in all the configurations.

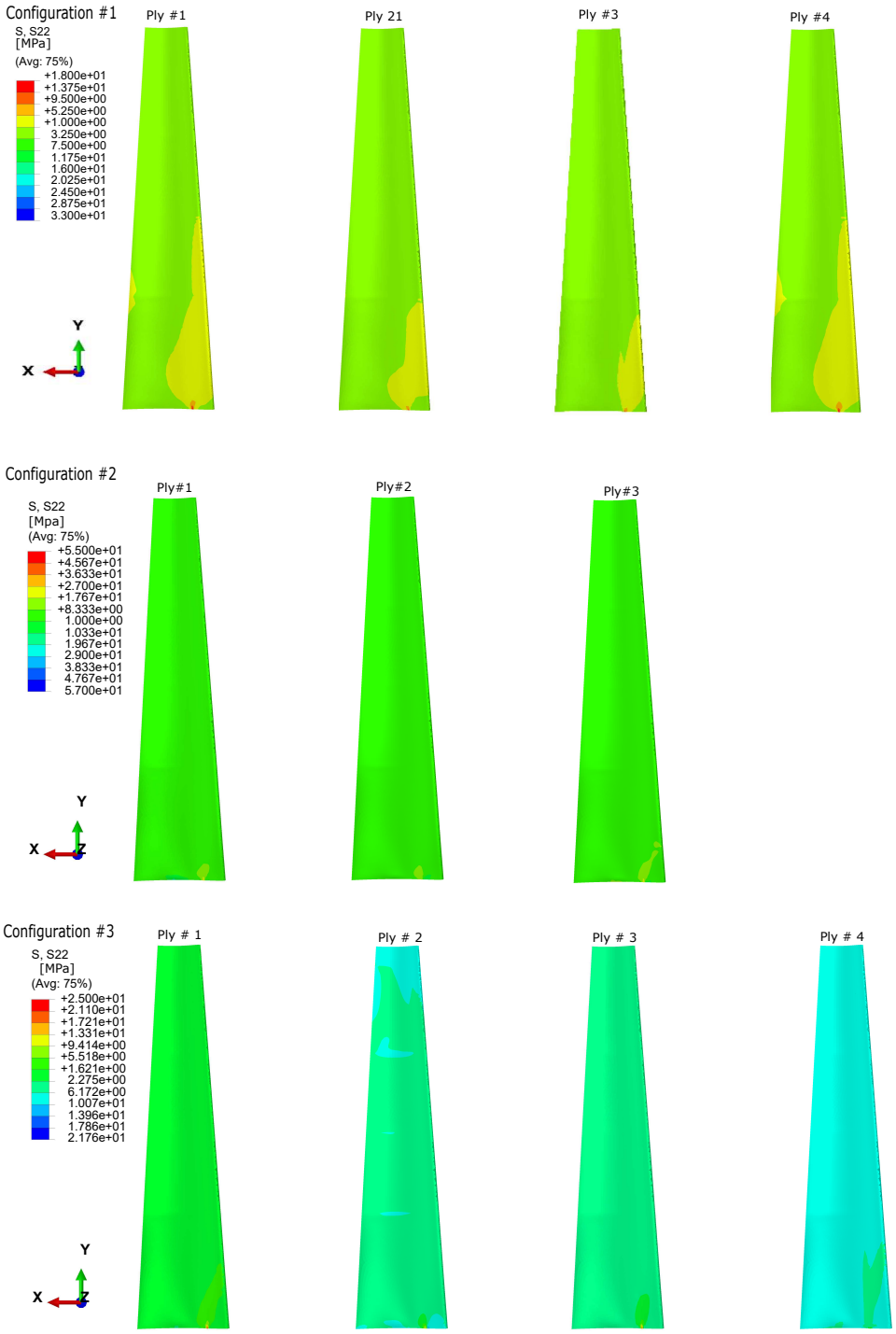

Figure 37. Stress S22 bottom surface

6.2.1. Tsai-Wu criterion

The Tsai-Wu criterion is a failure theory for orto-tropic materials like composites, the criteria represent in a graphical way a elliptical surface of failure with the S11 and S22 in the principal axis [9].

The material used for the analysis is the M6/SC1081 carbon fiber with epoxy resin. Using the properties given in the Daniel Ishai is obtained the Tsai-Wu expression for this specific material.

The figure (38) is the graphic representation of the criteria, this figure is product of the following expression:

$$F_1\sigma_1 + F_2\sigma_2 + F_{66}\sigma_6^2 + F_{11}\sigma_1^2 + F_{22}\sigma_2^2 + 2F_{12}\sigma_1\sigma_2 = 1 \tag{8}$$

It should be noted that the Tsai-Wu criterion is a 3d criteria as explained in [12] which means that the figure (38) that follow the equation (8) is the simplified way with σ_{66} = 1 that represent the biggest failure ellipse.

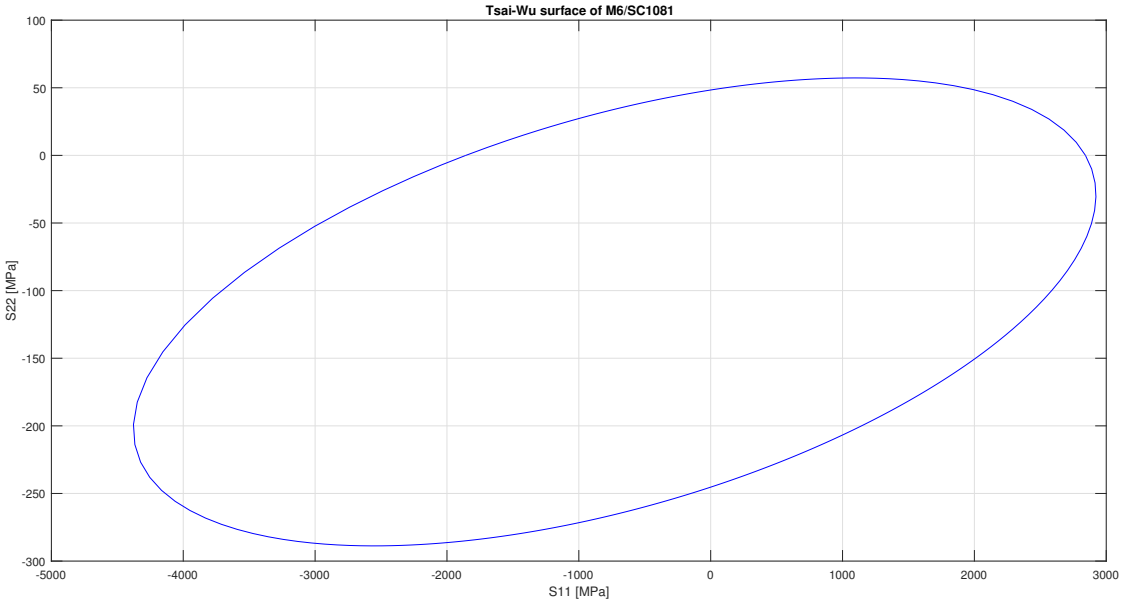

Figure 38. Tsai-Wu surface for M6/SC1081 with σ_{66}= 0

For each configuration was obtained the values of S11 and S22 for each node of the model using a Python routine, this values were plotted in the ellipse for each configuration. For each configuration it was obtained the critical value of S12 which represents the value of σ_{66}, this value makes the ellipse to be smaller and restricts the failure surface,that is why in the figures(40,41,42) have 2 ellipses. One represent the biggest when F=1 and the other is the critical one using the S_12 values.

Since the model is a composite modeled as a shell and most of the elements are cquad4 with normal integration each element have 4 integration points.

The configuration 1 and 3 counts with 1043196 values for S11, S22 and S12. The configuration 2 in consequence of the missing layer have significant less values 819654 for the whole model.

497 In the figure (39) is plotted all the configurations results in the maximum S12 and in figures
498 (40,41,42) is showed separately each surface and points using the critical S12 of the model.

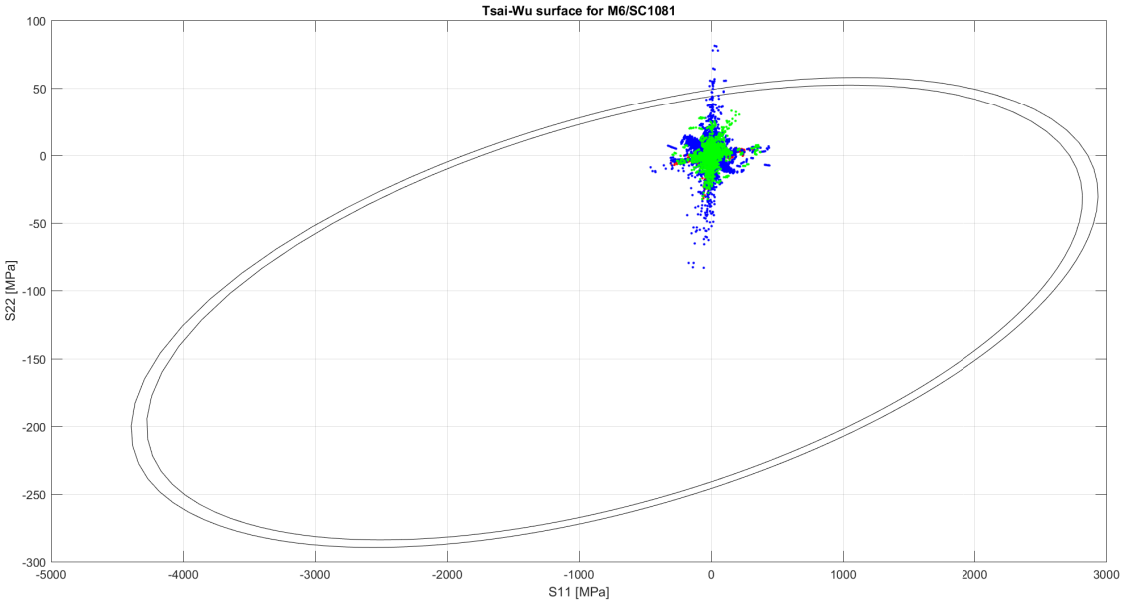

Figure 39. Tsai-Wu surface for M6/SC1081 for all configurations and maximum σ_{66}=35.1

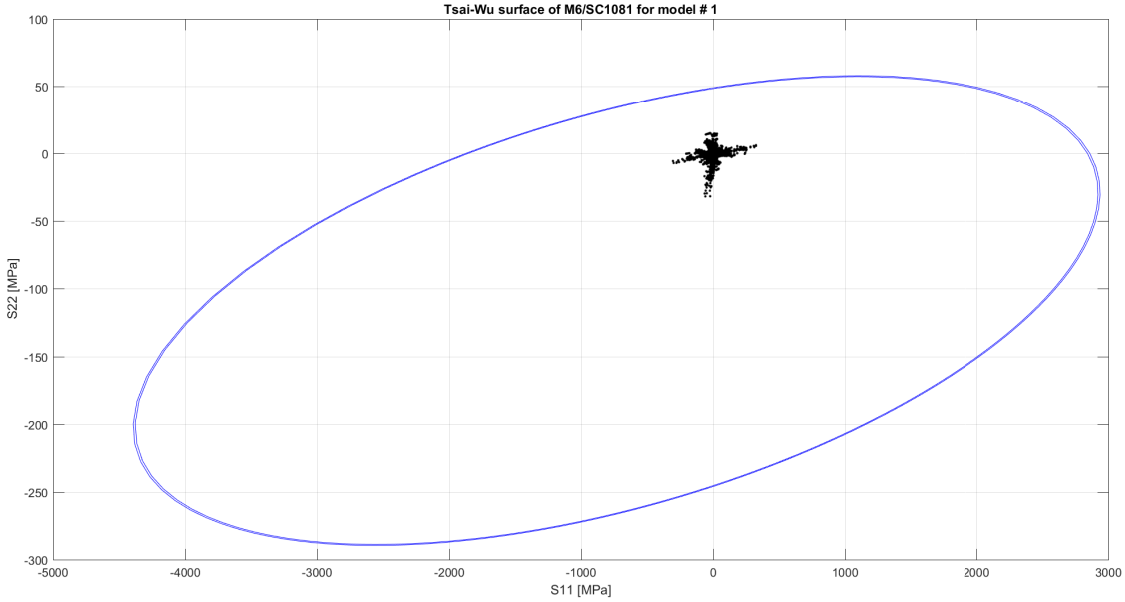

Figure 40. Tsai-Wu surface for M6/SC1081 for configuration 1 and σ_{66}=13.7

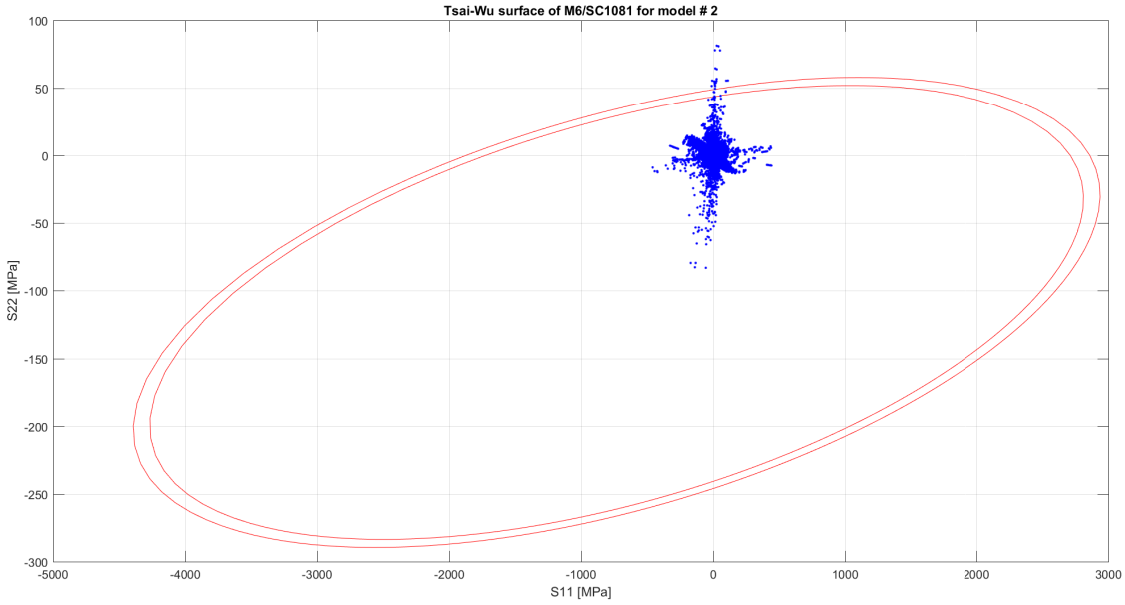

Figure 41. Tsai-Wu surface for M6/SC1081 for configuration 2 and σ_{66}=35.1

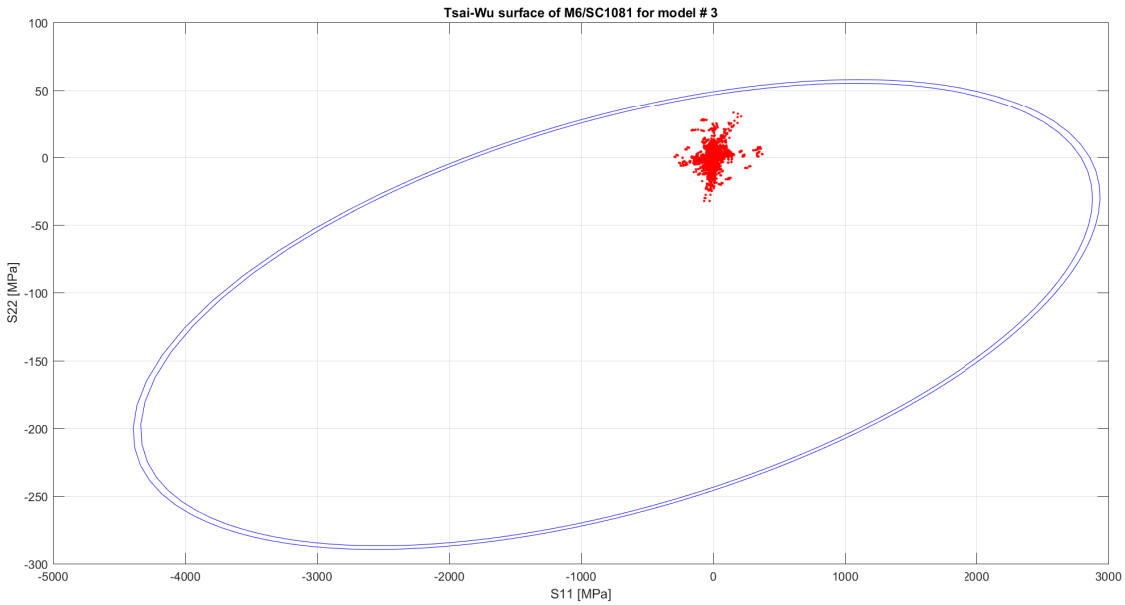

Figure 42. Tsai-Wu surface for M6/SC1081 for configuration 3 and σ_{66}=28.3

6.2.2. Margin of safety

Calculating the factor of Tsai-Wu (F) with the equation (8) for each value of the results. This F represents the criterion in all elements of model.

Using the values (F) is obtained the higher and lower for each model, to proceed with the calculation of the Margin of safety. The margin represent the endurance of the weakest and strongest element in the structure. This calculation is done using the equation (9).

$$M_s = \frac{1}{F} - 1 \tag{9}$$

The results in the Margin of safety are presented in the table (9), is also presented the values of (F).

	Configuration 1	Configuration 2	Configuration 3
Max F	0.5994	1.9441	0.6687
Min F	0.0260	0.028	0.0205
Max M.S	37	40.9	47.8
Min M.S	0.66	-0.485	0.4954

Table 9. Margin of safety

7. Conclusions

In this work an structural analysis of the Urcunina wing have been carried out. Using the aerodynamic design and posterior CFD simulations was obtained the information to do a Finite Element Analysis. From the FEA was obtained data that was validated with displacements and failure

theories to obtain the final design.

The original structure satisfy the design requirements of stress, displacements and failure criteria. The structure proposed suffer a 2.591 [mm] displacement with 0.07 of deflection in the tip that does not represent a plastic deformation and commitment of the structure.

The conf. 1 presented the most adequate results due to the stress nodal results of this configuration remain inside of the ellipse in the Tsai-Wu criteria. These values represent a margin of safety > 0 and means no failure

The conf. 3 also remain into the failure surface but the conf. 1 obtain lower stress and displacements results. The conf. 2 present failure in critical zones and considerable displacements.

A weight estimation was used for the initial design and even when the material is a composite the real mass of the structure exceed the estimation in 1.5 kg resulting in a 6 kg wing.

The reduction of weight in the structure is possible using other composite material combination, multi spar philosophy or rib reduction.

Abbreviations

The following abbreviations are used in this manuscript:

FEA	Finite Element Analysisis
CFD	Computational Fluid Dinamics
FEM	Finite Element Method
UAV	Unmaned Aerial Vehicle
VANT	Vehiculo Aereo no Tripulado
CFC	Carbon Fiber Composite
T.E	Trailing Edge
A.T	Attack Edge
U.S	Upper Surface
L.S	Lower Surface

1. Bravo-Mosquera, P.D.; Botero-Bolivar, L.; Acevedo-Giraldo, D.; Cerón-Muñoz, H.D. Aerodynamic design analysis of a UAV for superficial research of volcanic environments. *Aerospace Science and Technology* **2017**, *70*, 600–614. doi:10.1016/j.ast.2017.09.005.
2. McNutt, S.R. Seismic monitoring and eruption forecasting of volcanoes: a review of the state-of-the-art and case histories. In *Monitoring and mitigation of volcano hazards*; Springer, 1996; pp. 99–146.
3. Darmawan, H.; Walter, T.R.; Brotopuspito, K.S.; Subandriyo.; I Gusti Made Agung Nandaka. Morphological and structural changes at the Merapi lava dome monitored in 2012–15 using unmanned aerial vehicles (UAVs). *Journal of Volcanology and Geothermal Research* **2018**, *349*, 256–267. doi:10.1016/j.jvolgeores.2017.11.006.
4. McGonigle, A.J.S.; Aiuppa, A.; Giudice, G.; Tamburello, G.; Hodson, A.J.; Gurrieri, S. Unmanned aerial vehicle measurements of volcanic carbon dioxide fluxes. *Geophysical Research Letters* **2008**, *35*, 3–6. doi:10.1029/2007GL032508.
5. Narayan, A. Conceptual Design of a Carbon-fibre Composite Aircraft And Finite Element Analysis of the Wing. PhD thesis, Brunel University, West London, 2009.
6. Lima de Sousa, E.B. Projeto estrutural da asa de vant em material composito. PhD thesis, Instituto Tecnologico de Aeronáutica ITA, 2011.

7. Nicolás Castro, J.; Coronado, W.D.; Eduardo, L. Diseño estructural del fuselaje, ala central y union ala-fuselaje para la aeronave no tripulada (UAV) experimental SKYCRUISER X-1. PhD thesis, Universidad San Buenaventura, 2013.
8. Mazhar, F.; Khan, A.M. Structural Design of a Uav Wing Using Finite. *Science And Technology* **2010**, pp. 1–12. doi:AIAA 2010-3099.
9. Daniel, I.; Ishai, O. *Mechanics of Composite Materials*; 1970; pp. 881–886. doi:10.1016/B978-0-08-006421-5.50049-6.
10. Svensson, N.; Shishoo, R.; Gilchrist, M. Composite Materials. doi:10.1177/089270579801100102.
11. Soutis, C. Carbon fiber reinforced plastics in aircraft construction. *Materials Science and Engineering A* **2005**, *412*, 171–176. doi:10.1016/j.msea.2005.08.064.
12. Sebastián, E.C. Análisis de criterios de fallo para materiales compuestos. PhD thesis, Universidad Politecnica de Valencia, 2016.
13. element method, H. Explanation of the Finite Element Method, 2016.
14. Alcaraz, D. Diseño estructural y construcción de un avión no tripulado : El Proyecto Céfiro. PhD thesis, Universidad de Sevilla, 2015.
15. Rodrigues, L.E.M.J.; Queiroz, F.F. Aspectos teóricos para o cálculo e traçado do diagrama v-n de manobra e de rajada para uma aeronave destinada a participar da competição SAE-Aerodesign . *AeroDesign Magazine* **2009**, *1*, 1–5.